High Temp. Mater. Proc., Vol. **31** (2012), pp. 173–179 DOI 10.1515/htmp-2012-0013

Contact Strength and Cracking of Laminar Ceramics

Lucia Hegedűsová[1] **and Ladislav Ceniga**[1,*]

[1] Institute of Materials Research, Slovak Academy of Sciences, Košice, Slovak Republic

Abstract. The paper deals with the determination of strength of laminar ceramics by mechanical tests in bending and contact modes. The bending and contact modes are simulated by the four-point bending test, and by single-cycle contact test using rollers or spheres, respectively. In general, the determination of strength of ceramic materials results from statistical methods which are usually represented by the Weibull analysis. The Weibull analysis comprises the determination of the characteristic strength σ_0 and Weibull modulus m. The characteristic strength $\sigma_{0,\text{bend}}$ and $\sigma_{0,\text{cont}}$ as well as the Weibull moduli m_{bend} and m_{cont}, which are related to the four-point bending test and the single-cycle contact test using rollers, are thus determined, respectively. The comparison of numerical results of $\sigma_{0,\text{bend}}/\sigma_{0,\text{cont}}$, $m_{\text{bend}}/m_{\text{cont}}$ confirms the validity of the Fett's theory. Along with this verification, a microstructural analysis of strength-degrading defects which represent fraction origins is performed for both modes. The determination of the mechanical loading which causes material failure along with an analysis of parameters of cracks are also presented. The contact test using the spheres is also performed at a multi-cycle mode. The mechanical tests were applied to Al_2O_3-ZTA laminar ceramics (ZTA = $60\%Al_2O_3 + 40\%ZrO_2$).

Keywords. Ceramics, strength, fracture, defects, Weibull analysis.

PACS®(2010). 62.20.Mk, 81.05.Je, 81.40.Np, 81.70.Bt, 83.80.Ab.

1 Introduction

Conventional tests for the determination of strength of ceramic materials (three-/four-point bending tests) describe such failure behaviour which is related to simple stress states. This simple stress states mostly comprise of uniaxial stresses with relatively insignificant stress gradients. Mechanical loading within practical applications often leads to significantly inhomogeneous and multi-axial stress states [1–3] which can be simulated by contact line or point loading. The contact line and point loading is induced by two opposite rollers and two opposite spheres, respectively. In general, strength of ceramic materials is affected by the presence of flaws in a form of pores which originate during the material processing. The flaws are then a reason of material fracture and failure.

Due to the presence of the processing flaws, the determination of strength of ceramic materials is thus required to results from statistical methods, usually represented by the Weibull analysis [4–6]. This analysis determines the characteristic strength $\sigma_{0,\text{bend}}$ and $\sigma_{0,\text{cont}}$ along with the Weibull moduli m_{bend} and m_{cont}, which are related to the bending and contact modes, respectively. Additionally, the determination of $\sigma_{0,\text{cont}}$, m_{cont} considers the Fett's theory [7–9] which is valid for the four-point bending and single-cycle contact test using rollers.

Conversely, the contact mode performed by spheres induces cone cracks as a reason of material failure. Additionally, stable growth of the cone cracks is assumed to be a reason of higher values of $\sigma_{0,\text{cont}}$, m_{cont} compared with lower ones of $\sigma_{0,\text{bend}}$, m_{bend}. Accordingly, the higher values of m_{cont} correspond to significant preciseness of the determination of strength of ceramic materials. The contact test performed by spheres thus enables to obtain reproducible results. On the one hand, the determination requires large amount of specimens. On the other hand, the specimens are of small dimensions what is an advantage of this experimental technique which is thus suitable for new developed ceramic materials.

Aims of this paper are as follows:

1. an application of the Weibull analysis for the four-point bending and single-cycle contact tests using rollers or spheres to laminar ceramics.
2. experimental verification of the Fett's theory in case of the laminar ceramics.
3. a microstructural analysis of strength-degrading defects as fraction origins.
4. a fractographical analysis of cracks induced by the contact modes.
5. the determination of the mechanical loading which is a reason of material failure.
6. the determination of crack parameters at the single- and multi-cycle contact test using spheres.

* **Corresponding author:** Ladislav Ceniga, Institute of Materials Research, Slovak Academy of Sciences, Watsonova 47, 040 01 Košice, Slovak Republic; E-mail: lceniga@yahoo.com, lceniga@imr.saske.sk.

Received: September 6, 2011. Accepted: December 20, 2011.

In general, ceramics exhibits low tensile strength. Low tensile strength can be increased by the presence of such material components, e.g. precipitates, fibres, whiskers, which induced compressive thermal stresses in a matrix. These compressive thermal stresses represent a resistance against tensile mechanical loading.

The same is also valid in case of laminar ceramics with $2n + 1$ layers ($n \geq 1$). As an example, let laminar ceramics with $n = 1$ be considered, where α_{outer} and α_{inner} represent thermal expansion coefficients of outer and inner layers, respectively. If $\alpha_{\text{outer}} < \alpha_{\text{inner}}$, then the two outer layers and the inner layer are loaded by compressive and tensile thermal stresses which act in a plane of these layers. The compressive thermal stresses acting in this laminar ceramic system ($n = 1$) represent a resistance against tensile mechanical loading.

The bending and contact strength tests mentioned above are applied to the Al_2O_3-ZTA laminar ceramics, where ZTA $= 60\%Al_2O_3 + 40\%ZrO_2$ (mass %), and $n = 4$. This laminar system consists of regularly alternating five layers of Al_2O_3 and four layers of ZTA. In this case, the Al_2O_3 and ZTA layers are acted by compressive and tensile thermal stresses, respectively, due to $\alpha_{Al_2O_3} = \alpha_{\text{outer}} = 8.1\times10^{-6}\,\text{K}^{-1}$, $\alpha_{ZrO_2} = 10.3\times10^{-6}\,\text{K}^{-1}$, $\alpha_{\text{ZTA}} = \alpha_{\text{inner}} = 0.6 \times \alpha_{Al_2O_3} + 0.4 \times \alpha_{ZrO_2} = 8.98 \times 10^{-6}\,\text{K}^{-1}$ [10], and then $\alpha_{\text{outer}} < \alpha_{\text{inner}}$.

2 Experimental Procedure

The four-point bending test performed by the testing machine Lloyd LR 5KPLUS for $S_1 = 40$ mm, $S_2 = 20$ mm, $3 \times 4 \times 45$ [mm] was applied to specimens with the dimensions $W \times t \times L$ at room temperature and the loading rate 0.5 mm min^{-1}, where S_1 and S_2 are outer and inner spans, respectively. The characteristic strength $\sigma_{0,\text{bend}}$ is determined by the Weibull analysis [4, 5] which considers the stress σ_{bend}, as a function of the load P, derived as [6]

$$\sigma_{\text{bend}} = \frac{3P\,(S_1 - S_2)}{2tW^2}. \tag{1}$$

The fixture which is used for the contact test using rollers with the diameter D is shown in Figure 1 [7–9], where the two rollers 1 of standard hardened steel with the diameter $D = 3$ mm are pressed onto the specimen 2 with the load P. The testing machine Lloyd LR 5KPLUS was applied to specimens with the dimensions $W \times t \times L = 3 \times 4 \times$ (10–15) [mm] at room temperature in a such way that the load P was increased with a loading rate of 0.5 mm min^{-1} up to the critical value P_c to cause failure of specimens. The characteristic strength $\sigma_{0,\text{cont},r}$ is determined by the Weibull analysis [4, 5] which considers the measured stress $\sigma_{\text{cont},r}$ in the form [7–9]

$$\sigma_{\text{cont},r} = \frac{0.98P}{tW}, \tag{2}$$

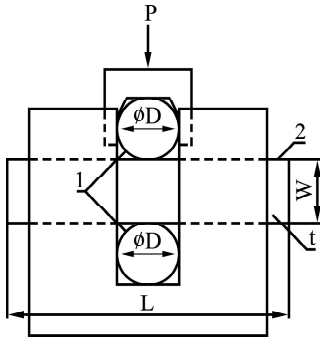

Figure 1. The fixture used for the contact test using rollers 1 with the diameter D applied by the load P to the specimen 2 with the dimensions $W \times t \times L$.

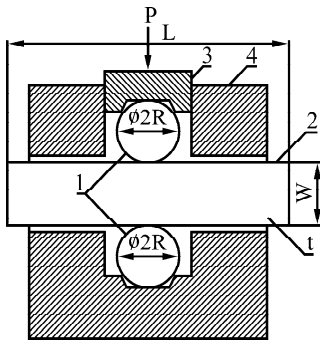

Figure 2. The fixture used for the contact test using spheres 1 with the radius R applied by the load P to the specimen 2 with the dimensions $W \times t \times L$, where P is transferred by the roller 3 guided by the hollow roller 4.

where P is load which causes failure of a material.

As published in [8, 9], the Fett's theory is represented by the following relationships

$$\sigma_{0,\text{bend},r} \approx \sigma_{0,\text{cont},r}, \quad m_{\text{bend},r} \approx 2m_{\text{cont},r}. \tag{3}$$

The fixture which is used for the single-cycle contact test using spheres of standard hardened steel with the radii $R = 2$; 2.5; 3.5 mm is shown in Figure 2 [7–9]. The specimen 2 is loaded via the two opposing spheres 1 by the load P. The load P is transferred to the upper sphere by the roller 3 guided by the hollow roller 4. The testing machine Lloyd LR 5KPLUS was applied at room temperature and a loading rate of 0.5 mm min^{-1} to specimens with the dimensions $3 \times 4 \times 25$ [mm] or to fragments of shorter length. A part of a number of specimens was tested by the load P increasing to the critical value P_c to cause failure of specimens. A rest of number of specimens was tested by an increasing load to be stopped at $P = 4.9$ kN reached before the critical value P_c, i.e. before failure of specimens, with an aim to investigate a character and parameters of cracks to originate during the loading. The specimens which are loaded without their failure were cut through a

centre of a contact surface, ground and polished due to optical and electron microscopy used for the determination of the length c of a crack and the angle α, where α is measured between a crack and the contact surface. The characteristic strength $\sigma_{0,\mathrm{cont},s}$ is determined by the Weibull analysis [4,5] which considers the measured stress $\sigma_{\mathrm{cont},s}$ in the form [8,9]

$$\sigma_{\mathrm{cont},s} = \frac{1-2\nu_m}{3\pi}\left[6P\left(\frac{E}{R}\right)^2\right]^{1/3}, \qquad \frac{1}{E} = \frac{1-\nu_s^2}{E_s} + \frac{1-\nu_m^2}{E_m}, \tag{4}$$

where E_s, ν_s and E_m, ν_m represent the Young's modulus, the Poisson's ratio for the spheres and an investigated ceramic material (see Table 1), respectively.

Material	E_m (GPa)	ν_m	E_s (GPa)	μ_s
Al_2O_3-ZTA	377	0.16	–	–
SHS	–	–	200	0.2

Table 1. Material parameters of the Al_2O_3-ZTA laminar ceramics and the standard hardened steel (SHS) of spheres.

The fixture in Figure 2 is also used for a multi-cycle mode at the radius $R = 2.5$ mm of the spheres. This multi-cycle mode was performed at room temperature, the frequency $f = 10$ Hz, the number $n = 10^2, 10^3, 10^4, 10^5$ of cycles, and the load P which was varied between $P_{\min} = 6$ kN and $P_{\max} = 20$ kN.

As mentioned above, these mechanical tests were applied to the Al_2O_3-ZTA laminar ceramics. This ceramics, made by tape casting which is followed by binder burnout and sintering, was prepared at the National Research Council, Institute of Science and Technology for Ceramics, Faenza, Italy, in a form of a plate with the dimensions $3 \times 42 \times 42$ [cm].

Specimens of a number of 10–30, used for the mechanical tests, were cut by diamond tools, consequently ground and polished with 1 μm finish, where their edges were chamfered to the radius 0.15 mm to minimize an stress concentration influence.

The sectioning for the microstructural analysis was performed by a power-driven diamond cut-off wheel. Two-step planar grinding realized by semi-automatic equipment was followed by mechanical polishing. The microstructural analysis was performed by optical and scanning electron microscopy, and grain size was determined by the software Image J.

A study of fracture surfaces was performed by optical and scanning electron microscopy. The fractographical analysis of specimens broken at the four-point bending test was applied for the determination of fracture origins represented by flaws which originates during the material processing. In case of the contact test using rollers, fracture paths could not be identified due to the destruction of specimens to pieces.

The specimens loaded without their failure were cut through a centre of a contact surface, consequently ground and polished due to optical and scanning electron microscopy. The microscopy was used for the determination of the crack length c and the angle α by the software Image J [11]. The angle α of the crack propagation was measured between the crack and the contact surface 2 in Figure 2.

3 Results and Discussion

Figure 3 show microstructure of the 9-layered Al_2O_3-ZTA laminar ceramics. The dark and bright components in Figure 3a represent the Al_2O_3 and ZTA layers with thickness of 193 μm and 529 μm, respectively. Microstructure of the ZTA layer shown in Figure 3b consists of relatively large Al_2O_3 grains and small ZrO_2 grains as dark and bright phases with size of 1 μm and 0.3 μm, respectively. The Al_2O_3 and ZrO_2 grains which both are of an equiaxed shape are uniformly dispersed throughout the ZTA layer. On the other hand, the Al_2O_3 grains with size of 3 μm (see Figure 3c) in the Al_2O_3 layer exhibit well-faceted boundaries and sharp triple points. Finally, the two layers, i.e. Al_2O_3 and ZTA layers, are well defined by straight interfaces (see Figure 3d). Additionally, no significant residual porosity is observed at these interfaces.

The characteristic strength $\sigma_{0,\mathrm{bend}}$, $\sigma_{0,\mathrm{cont},r}$, $\sigma_{0,\mathrm{cont},s}$, the Weibull moduli m_{bend}, $m_{\mathrm{cont},r}$, $m_{\mathrm{cont},s}$ [4, 5] along with $m_{\mathrm{bend}}/m_{\mathrm{cont},r}$, $\sigma_{0,\mathrm{cont},r}/\sigma_{0,\mathrm{bend}}$ for Al_2O_3-ZTA are presented in Table 2. Numerical values of $\sigma_{0,\mathrm{cont},s}$, $m_{\mathrm{cont},s}$ represent mean values of experimental results at different radii of the sphere, i.e. $R = 2$; 2.5; 3.5 mm.

As presented in Figure 3c, the Al_2O_3 layer exhibits grains with a diameter of 25–30 μm which is much greater than diameters $<$ 1 μm and 3–5 μm of the Al_2O_3 and ZrO_2 grains of the ZTA layer (see Figure 3b), respectively. Similarly, Figure 4 shows fracture surfaces of Al_2O_3-ZTA loaded by rollers of the single-cycle contact test, i.e. 3D stereomicroscopic micrograph (see Figure 4a), scanning electron micrograph (see Figure 4b), and the ZTA layer with the presence of an abnormal large flaw at the Al_2O_3-ZTA boundary (see Figure 4c).

Such flaws along with the large grains of Al_2O_3 in the Al_2O_3 layer might be assumed to be a reason of a deviation from the Fett's theory (see Eq. (3)) regarding the ratio $m_{\mathrm{bend}}/m_{\mathrm{cont},r} = 2.5$ (see Table 2) in contrast to the ratio $\sigma_{0,\mathrm{cont},r}/\sigma_{0,\mathrm{bend}} = 1.1$ which corresponds to the Fett's theory. Additionally, the Al_2O_3 and ZrO_2 layers are characterized by different thermal expansion coefficients. Consequently, thermal stresses acting in a plane of these layers exhibit a significant distribution along the normal of this plane. This

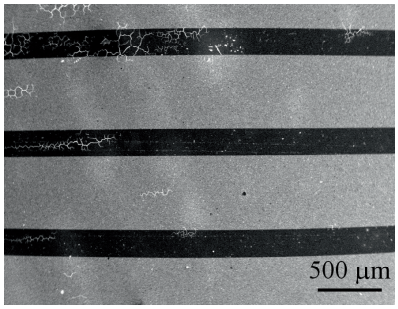

(a)

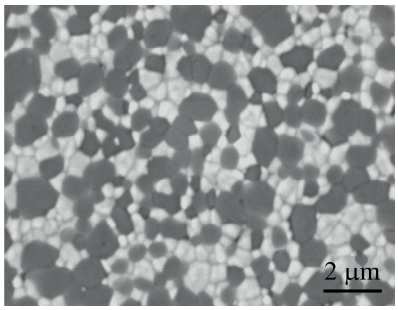

(b)

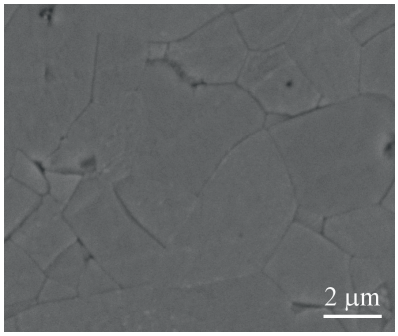

(c)

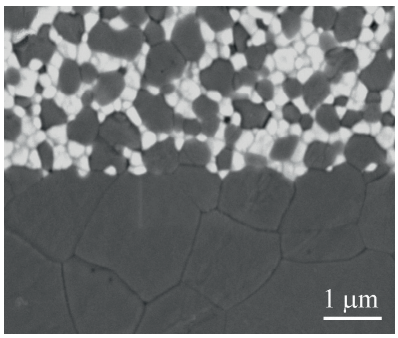

(d)

Figure 3. SEM micrographs of microstructure of the Al_2O_3-ZTA multi-layered composite: (a) low magnification (Al_2O_3 – dark layers, ZTA – bright layers), (b) ZTA $=$ 60 vol%Al_2O_3+40 vol%ZrO_2, (c) the Al_2O_3 layer, (d) the detail of an interface of Al_2O_3 and ZTA layers.

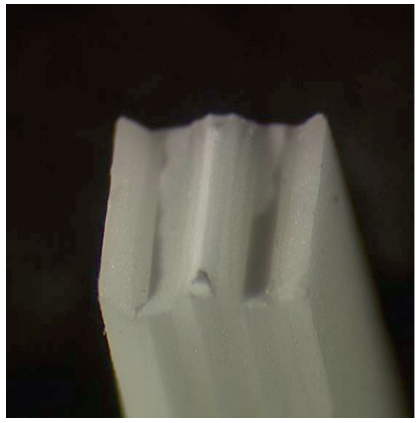

(a)

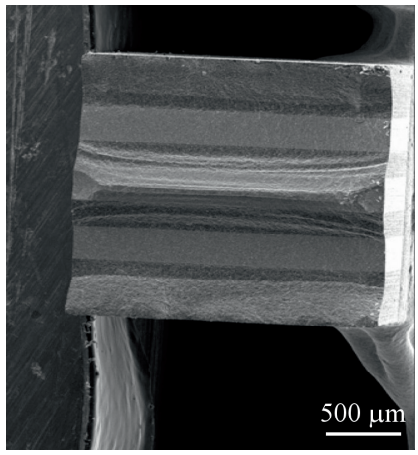

(b)

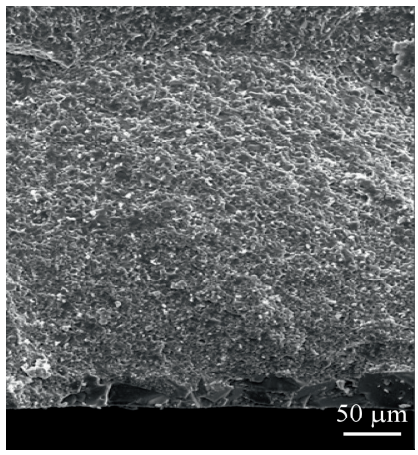

(c)

Figure 4. Fracture surfaces of the Al_2O_3-ZTA laminar ceramics loaded by rollers in the single-cycle contact test: (a) 3D stereomicroscopic micrograph of Al_2O_3-ZTA, (b) scanning electron micrograph of Al_2O_3-ZTA, (c) scanning electron micrograph with a fracture origin on a tensile surface of Al_2O_3-ZTA.

$\sigma_{0,\text{bend}}$ (MPa)	$\sigma_{0,\text{cont},r}$ (MPa)	$\sigma_{0,\text{cont},s}$ (MPa)	$\sigma_{0,\text{cont},r}/\sigma_{0,\text{bend}}$
650	715	3453.3	1.1
m_{bend}	$m_{\text{cont},r}$	$m_{\text{cont},s}$	$m_{\text{bend}}/m_{\text{cont},r}$
19.8	7.9	21.6	2.5

Table 2. The characteristic strength $\sigma_{0,\text{bend}}$, $\sigma_{0,\text{cont},r}$ and $\sigma_{0,\text{cont},s}$ along with the Weibull moduli m_{bend}, $m_{\text{cont},r}$ and $m_{\text{cont},s}$ related to the four-point bending test, the single-cycle contact test using rollers and spheres, respectively, where $\sigma_{0,\text{cont},s}$ and $m_{\text{cont},s}$ represent average values of experimental values determined at the radii $R = 2, 2.5, 3.5$ mm.

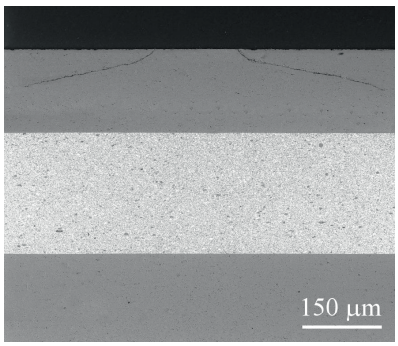

Figure 5. SEM micrograph of a cross-section view with a cone crack induced by the single-cycle contact test using spheres with the radius $R = 2.5$ mm, where the crack length $c = 280$ µm, the crack angle $\alpha = 26.5°$, and the contact surface radius $R_{\text{cs}} = 80$ µm.

distribution might be assumed to be also a reason of the deviation from the Fett's theory.

Due to $m_{\text{cont},s} > m_{\text{cont},r}$, the single-cycle contact test using spheres might be thus assumed to represent the most precise and considerable for the determination of strength of ceramic materials. Additionally, with regard to $\sigma_{0,\text{cont},s} > \sigma_{0,\text{bend}}$, $\sigma_{0,\text{cont},s} > \sigma_{0,\text{cont},r}$, the preciseness can be explained by stable growth of cone cracks [12], and not by an initial size of processing flaws. As presented in [12], the cone cracks propagate from the contact surface with a quasi-perpendicular course to the contact surface (5–10 µm). As shown in Figure 5, this perpendicular course is then followed by a linear course (250–300 µm). The cone crack in Figure 5 is related to the single-cycle contact test at the radius $R = 2.5$ mm of the spheres, where the crack length $c = 280$ µm, the crack angle $\alpha = 26.5°$, and the contact surface radius $R_{\text{cs}} = 80$ µm.

As shown in Figure 6a, the critical load P_c as a reason of failure of a specimen is an increasing function of the radius $R = 2; 2.5; 3.5$ mm of spheres. A smaller radius which results in a smaller contact surface is a reason of a higher "concentration" of stresses, i.e. higher gradients of stresses

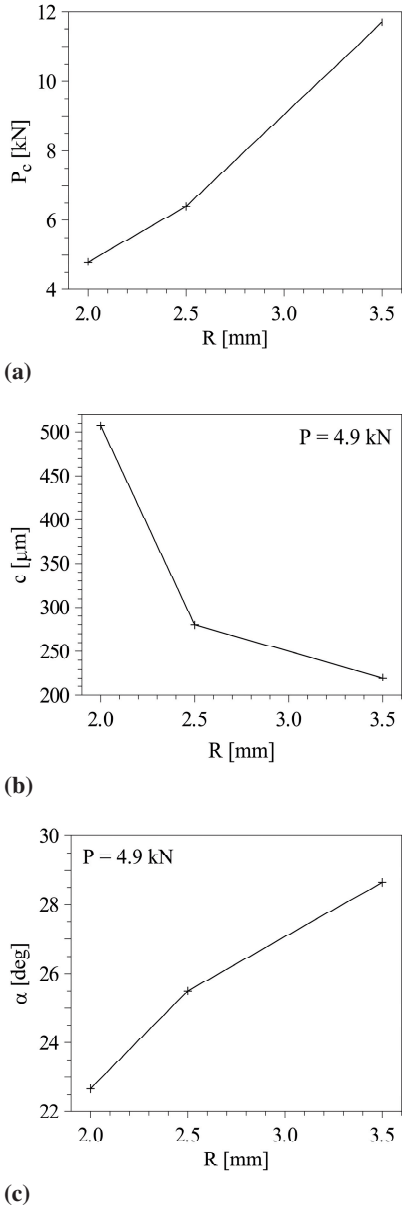

Figure 6. The critical load P_c, the crack length c, and the angle α versus the radius $R = 2, 2.5, 3.5$ mm of the spheres of the single-cycle contact test, where c, α are determined at the load $P = 4.9$ kN.

induced in a specimen by the load P. The higher gradients are assumed to result in a lower value of P_c, and vice versa. Additionally, smaller gradients at higher R are a reason of a more homogeneous stress state close to the normal to a contact surface, where the normal is related to a centre of the contact surface. Finally, the crack length $c = c\,(R)$ and the angle $\alpha = \alpha\,(R)$ (see Figure 6b, c) represent decreasing and increasing functions of $R = 2; 2.5; 3.5$ mm, respectively.

Figure 7 shows the primary (p) and secondary (s) cone cracks which are formed during the multi-cycle contact test using spheres with the radius $R = 2.5$ mm at the number

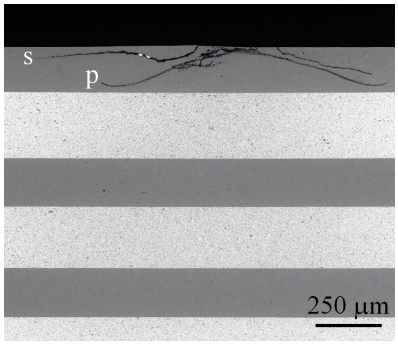

Figure 7. SEM micrographs of cross-section of the Al_2O_3-ZTA laminar ceramics loaded by the multi-cycle contact test using spheres with the radius $R = 2.5$ mm at the number $n = 10^5$ of cycles: the primary (p) and secondary (s) cone cracks.

$n = 10^5$ of cycles. In contrast to Figure 5, the primary cone crack exhibits significant kinks.

Figure 8a shows the crack length $c = c\,(n, R)$ as an increasing function of the number n of cycles, where R represents a parameter of this function. The increase of c is less significant at a higher value of n than at a lower value of n, i.e. the tangent dc/dn is a decreasing function of n as analytically determined in [13]. Contrarily, as shown in Figure 8b, $\alpha = \alpha\,(n, R)$ represents a decreasing function of n. The functions $c = c\,(n, R)$, $\alpha = \alpha\,(n, R)$ are related to the primary cone crack (see Figure 7).

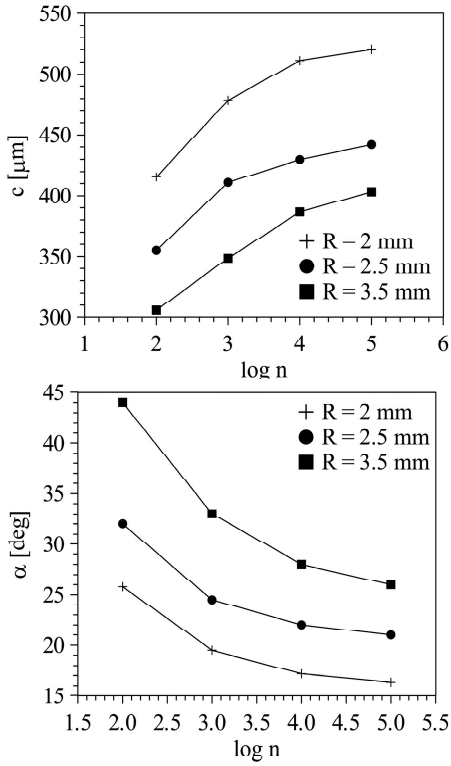

Figure 8. The length c and the angle α of the primary cone crack (see Figure 7) as functions of the number n of cycles of the multi-cycle contact test using spheres with the radii $R = 2, 2.5, 3.5$ mm

4 Conclusions

With regard to the aims presented in Section 1 (see Items 1–6), results of the four-point bending and contact tests are as follows:

1. The presence of large processing flaws at the Al_2O_3-ZTA boundary along with the significant distribution along the normal of a plane of Al_2O_3-ZTA might be assumed to be reasons of the deviation from the Fett's theory (see Eq. (3)) regarding the ratio $m_{\text{bend}}/m_{\text{cont},r} = 2.5$ (see Table 2).
2. Due to $m_{\text{cont},s} > m_{\text{cont},r}$ (see Table 2), the single-cycle contact test using spheres might be assumed to represent the most precise and considerable for the determination of strength of ceramic materials. Additionally, due to $\sigma_{0,\text{cont},s} > \sigma_{0,\text{bend}}$, $\sigma_{0,\text{cont},s} > \sigma_{0,\text{cont},r}$, the preciseness can be explained by stable growth of cone cracks [12], and not by an initial size of processing flaws.
3. The critical load which is a reason of material failure, the crack length, and the crack angle represent increasing, decreasing and increasing functions of a radius of the spheres at the single-cycle contact test, respectively.
4. In contrast to the single-cycle contact test, the multi-cycle contact test leads to the formation of multi-cone cracks, i.e. primary and secondary cone cracks.
5. In case of the multi-cycle contact test using the spheres, the length and angle of the primary cone crack represent increasing and decreasing functions of a number of cycles, respectively.

Acknowledgments

This work was supported by the Slovak Research and Development Agency under the contracts No. APVV-0034-07, No. COST-0042-06, No. COST-0022-06, No. APVV-51-061505, No. APVV-0171-06; by the Slovak Grant Agency VEGA (2/0156/10, 2/0120/10); by HANCOC: MNT.ERA-NET 01/2009-12/2011.

Authors are thankful to Dr. Goffredo de Portu from Institute of Science and Technology for Ceramics, Faenza, Italy, for providing the experimental material.

References

[1] J. Dusza and M. Steen, Microhardness load size effect in individual grains of a gas pressure sintered silicon nitride, *Journal of the American Ceramic Society* **81** (1998), 3022–3024.

[2] J. Dusza, P. Šajgalík and M. Steen, Fracture toughness of a silicon nitride/silicon carbide nanocomposite at 1350 C, *Journal of the American Ceramic Society* **82** (1999), 3613–3615.

[3] T. Lube and J. Dusza, A silicon nitride reference material – a testing program of ESIS TC6, *Journal of the European Ceramic Society* **27** (2007), 1203–1209.

[4] W. Weibull. *A Statistical Theory of the Strength of Materials*, Generalstabens Litografiska Anstalts Förlag, Stockholm, 1939.

[5] EN 843-5 Advanced technical ceramics – Mechanical properties of monolithic ceramics at room temperature – Part 1: Statistical analysis, CEN, 2006.

[6] EN 843-1 Advanced technical ceramics – Mechanical properties of monolithic ceramics at room temperature – Part 1: Determination of flexure strength, CEN, 2006.

[7] T. Fett, E. Ernst, D. Munz, D. Badenheim and R. Oberacker, Weibull analysis of ceramics under high stress gradients, *Journal of European Ceramic Society* **23** (2003), 2031–2037.

[8] T. Fett and D. Munz, Influence of stress gradients on failure in contact strength tests with cylinder loading, *Engineering Fracture Mechanics* **69** (2002), 1353–1361.

[9] T. Fett, E. Ernst and D. Munz, Contact strength measurements of bars under opposite sphere loading, *Journal of Materials Science Letters* **17** (2002), 2912–2920.

[10] `http://accuratus.com/`.

[11] `http://rsbweb.nih.gov/ij`.

[12] T. Fett, E. Ernst and D. Munz, Contact strength measurements of bars under opposite sphere loading, *Journal of Materials Science Letters* **21** (2002), 1955–1957.

[13] T. Fett, E. Ernst, G. Rizzi, D. Munz, D. Badenheim and R. Oberacker, Sphere contact fatigue of a coarse-grained Al_2O_3 ceramic, *Fatigue and Fracture of Engineering Materials and Structures* **29** (2006), 876–886.